

Article

Conceptualising a Hybrid Flying and Diving Craft

Keith F. Joiner ¹  and Ahmed A. Swidan ^{2,3,*} 

¹ Capability Systems Centre, University of New South Wales, Australian Defence Force Academy, Canberra 2600, Australia; k.joiner@adfa.edu.au

² Arab Academy for Science, Technology and Maritime Transport, Alexandria 21913, Egypt

³ School of Engineering and Technology, University of New South Wales, Australian Defence Force Academy, Canberra 2600, Australia

* Correspondence: a.swidan@unsw.edu.au

Abstract: This paper introduces the conceptual design of a submersible seaplane that merges the maturity of the wing-in-ground (WIG or ekranoplan) crafts and seaplanes with covert hybrid underwater insertion, travel, and recovery. WIG crafts have a higher lift-to-drag ratio and thus improved endurance, while hybrid crafts have recently become feasible due to advances in materials, electric propulsion, and multi-medium computational fluid dynamics. The reconnaissance design can insert, loiter, and extract from underwater surfaces if necessary; it can fly in or out of ground effect, keep watch on the sea surface while recharging, and travel underwater. This design minimizes Doppler and infrared signatures to evade the surface wave, backscatter radar systems, and cube satellite arrays typical in contested maritime areas. Five critical enabling technologies are overviewed, showing how they enable a conceptual design. This project was conducted in collaboration with two industrial partners, namely Ron Allum and Thales Australia. The conceptual design has been socialised and confirmed at technical conferences from each core discipline and partly confirmed by a recent Chinese design and testing of a similar hybrid uncrewed aerial vehicle (HUAV). Recommendations are made for improving the conceptual design before proof-of-concept prototype testing. Given the seminal nature of HUAV design and research and some of the unique innovations proposed, the lessons learned from this iteration will likely be significant to other designers and researchers.



Citation: Joiner, K.F.; Swidan, A.A. Conceptualising a Hybrid Flying and Diving Craft. *J. Mar. Sci. Eng.* **2023**, *11*, 1541. <https://doi.org/10.3390/jmse11081541>

Academic Editor: Alon Gany

Received: 6 July 2023

Revised: 27 July 2023

Accepted: 31 July 2023

Published: 2 August 2023



Copyright: © 2023 by the authors. Licensee MDPI, Basel, Switzerland. This article is an open access article distributed under the terms and conditions of the Creative Commons Attribution (CC BY) license (<https://creativecommons.org/licenses/by/4.0/>).

1. Introduction

The study of small Uncrewed Aerial Vehicles (UAVs) for intelligence operations has been an area of interest for quite some time [1]. When these studies are coupled with the use of wing-in-ground (WIG) for a higher lift and fuel efficiency and the possibility of a subsurface launch and recovery, the resultant aircraft can potentially change how underwater pipes can be inspected and/or how militaries will gather intelligence. The developed Low-Observable Submersible WIG Craft for Electronics Intelligence (LOSSEI) is a hybrid UAV (HUAV) designed to be launched at sea, navigate underwater at low speeds, and also conduct intelligence gathering operations over several days while solar recharging before resubmerging to be recovered again by the sea.

The LOSSEI project is a multi-year design exercise incorporating final-year engineering projects with industry support from Ron Allum Deepsea Services and Thales Avionics. This highly multidisciplinary project draws upon the research and findings of unpublished theses by two students in 2020, six further student theses in 2021, and lesser contributions in 2022. The conceptual design has been socialised and confirmed at technical conferences from each core discipline, including subsea [1], defence technology [2], computational fluid dynamics [3], and telecommunications [4]. There was some limited research literature on

hybrid uncrewed aerial vehicles that encouraged the beginning of this research work, such as a 2015 comprehensive survey [5], 2016 research into a power system [6], water entry analyses in 2016 [7] and 2017 [8], a design based upon computational fluid dynamics in 2017 [9], and some testing and characterisation in 2018 [10].

Over the last two years, and concurrent with our LOSSEI research, there has been a spate of Chinese publications documenting the design and testing of HUAVs, starting with the design fabrication and characterisation of a HUAV in 2021 [11], followed by 2022 research into lifting principles [12], a numerical simulation of air–water transition [13], further design, fabrication, and experimentation [14], cross-domain control [15], and a miniature low-cost HUAV [16]. Such work confirms that some technologies have progressed for HUAVs sufficiently for us to recommend substantive proof-of-concept testing for this and other such hybrid vehicles.

The reconnaissance mission and design are shown with dimensions in Figures 1 and 2, respectively, with an estimated mass of between 27 and 57 kg. The craft's missions are still evolving; however, it can insert, loiter, and extract from underwater surfaces if necessary, can fly in or out of ground effect, keep watch on the sea surface while recharging, and travel underwater. In addition, this design minimizes Doppler and infrared signatures to evade the surface wave, backscatter radar systems, and cube satellite arrays typical in contested maritime areas [17].

The LOSSEI craft has been designed with a NACA 4412 airfoil, because that airfoil has been used extensively for wing-in-ground effect research, albeit this airfoil has had recent minor improvements in the WIG effect [18,19]. LOSSEI was modelled using the popular industry package, Fusion 360, which was found relatively easy to use.

LOSSEI has been designed to remain buoyant on the water's surface, while maintaining an ideal clearance between the wing and the water for the WIG effect in still conditions (70 mm). Another design consideration affecting the buoyant geometry is the 25-degrees deadrise angle. These design values are justified in the water drop test computational fluid dynamics section and the wing-in-ground effect sections that follow. For example, the 25-degrees deadrise angle was conceptually selected based on the authors' past experience [20], aiming to minimise the corresponding transient slamming loads during landing, as lower deadrise angles, e.g., 15-degrees, would experience higher slam forces [21], while preserving a sufficient buoyancy to eliminate the prospect of diving if compared with higher deadrise angles, e.g., 30-degrees [22]. With these considerations integrated into the design, the main hull and demi-hulls had a displacement volume of 0.02668 m^3 , adequate to maintain the desired position on the water's surface. When the vessel is submerged, however, the displaced volume changes significantly. As LOSSEI is fully sealed during the surfacing evolution, the submerged displacement volume is equivalent to the entire geometric volume of the craft. This volume is calculated with Fusion 360 CAD software to be 0.1289 m^3 . This volume provides a buoyancy force of 1259.74 N in the positive (upwards) direction, 992.94 N greater than the calculated gravitational force of 266.8 N for the 27.2 kg craft. These calculations confirm that LOSSEI theoretically has enough buoyancy to surface under its own positive buoyancy effectively.

It is also essential to calculate the longitudinal centre of buoyancy (LCB) for the craft with this positive buoyancy. The LCB is used to determine the direction in which the vessel will pitch, due to the forces acting on it. For a fully submerged body, the LCB is equivalent to the centre of volume of the entire craft. For LOSSEI, this point is located 368.53 mm from the nose, which places it 180.29 mm in front of the craft's longitudinal centre of mass (LCM) (548.82 mm from the nose).

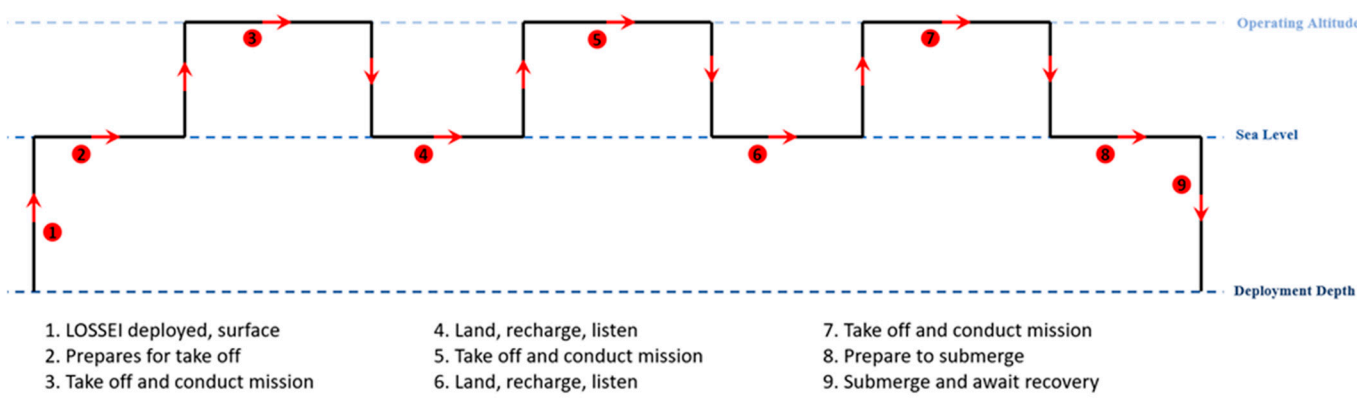


Figure 1. Indicative mission of Submersible WIG Craft [1].

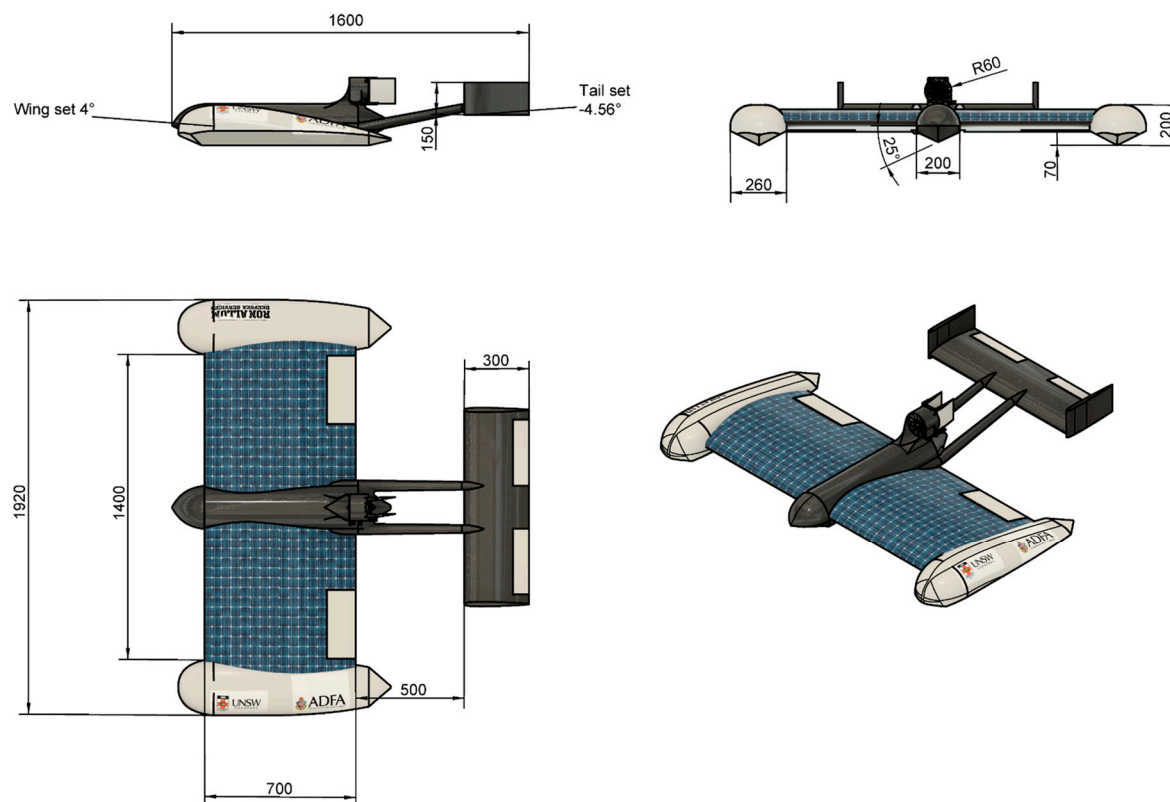


Figure 2. The conceptual design of a Submersible WIG Craft.

Five of the leading enabling technologies are overviewed in this article to show how they enable the design:

1. The wing-in-ground effect for an efficient high-endurance and low-speed cruise while staying very low to the water for a reduced Doppler signature;
2. Electric ducted fans from the developing drone market are powerful enough for take-off from the water and likely efficient in both above- and below-water cruises;
3. When merged with carbon fibre, new compressible syntactic foam materials can likely survive both compression depths and flying and landing forces;
4. Enhanced batteries and conformal solar panel recharging technologies;
5. Evolving computational fluid dynamics (CFD) packages can analyse both hydrodynamic and aerodynamic design performances.

2. Wing-in-Ground (WIG) Effect

Ground effect, or WIG, is a natural phenomenon of improved aerodynamic performance in marine aircraft operating near the water's surface. However, this effect is only evident when an aircraft is flying at a height less than the length of one wing chord [18] (2010), named by some researchers as the critical height [19].

The ground effect combines two aerodynamic phenomena: chord and span-dominated ground effect [23]. The chord-dominated ground effect increases the lift, by developing an extremely high-pressure air cushion on the airfoil's underside as it approaches the ground [24]. During WIG flight, the air on the wing's undersurface decelerates significantly, trapping the air between the ground and the wing and increasing the pressure. This air cushion is also known as the ram effect and can cause the air under the wing to stagnate if the clearance height reduces too much.

The span-dominated ground effect directly influences the induced drag of the airfoil. The wingtip vortices cannot fully develop at a low ground clearance, so the leakage from the underside of the wing is lower [18]. As a result, the dynamic cushion increases the effective span and the effective aspect ratio of an aircraft. The research documented by Qu et al. (2015) finds that the WIG effect declines with a reducing aspect ratio and that endplates can retain the WIG effect for lower aspect ratios, as used in our conceptual design.

Hiemcke [23] found that the ground effect phenomenon is only significant if the wing is within one chord length of the ground plane. He showed that at a maximum, the lift is increased by approximately 66 per cent when the height-to-chord ratio is 0.1 compared to the airfoil performance out of the WIG. Values of height-to-chord less than 0.25 have been referred to as an extreme ground effect, as these place the aircraft at a higher risk of impact and induce stability challenges [19].

The air cushion trapped by the ground effect is shown for the LOSSEI craft in Figure 3, at a height-to-chord ratio of 0.1 or 70 mm above water and a maximum endurance speed for this condition of 21 m/s.

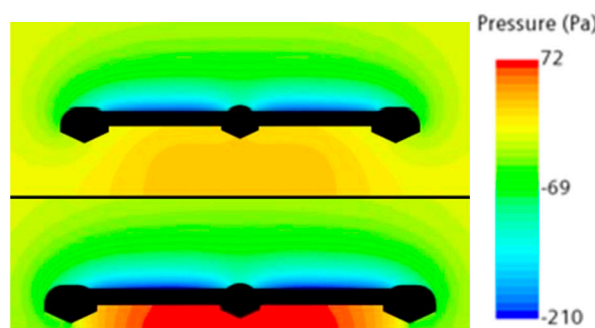


Figure 3. CFD of the LOSSEI craft in ground effect at the maximum endurance speed condition.

Research into the stability of the NACA 4412 [24] and the effect of surface waves by [25,26] has been extended by the research team, showing promise in the effect being sustained across waves, on average and with manageable perturbations from the wavelengths likely using laser-ranging altimeters. This aspect is discussed further later.

3. Electric-Ducted Fans (EDF)

The greatest challenge for the EDF is the take-off case. Due to the hydrodynamic drag, the thrust required for the LOSSEI to take off is significantly higher than that for a conventional UAV.

The thrust required to take off from flat water is modelled in Star CCM+ at six positions with fixed velocity and pitch angles, shown smoothed in Figure 4. The lift on the LOSSEI craft throughout the take-off cycle begins at a low speed, being dominated by the buoyancy force. As the velocity increases, the lift is dominated by hydrodynamic lift as the fuselage

and demi-hulls begin to plane on the water's surface. The end of the take-off sequence shows an aerodynamic lift, finally taking the LOSSEI into the air. Further details on the take-off case are covered later under CFD analyses.

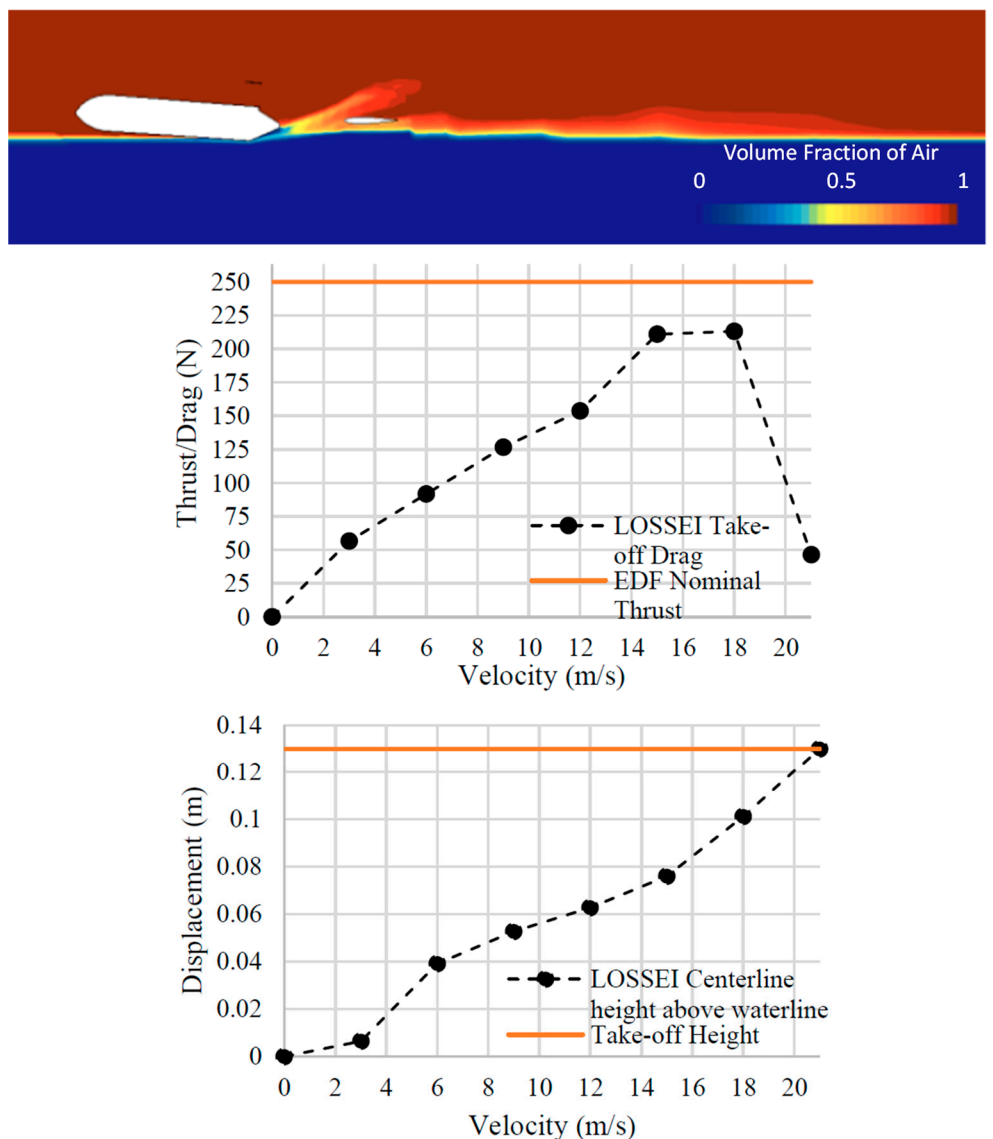


Figure 4. CFD of the LOSSEI craft in ground effect at the maximum endurance speed condition.

The EDF for the LOSSEI is intended to be an off-the-shelf unit. Therefore, an EDF that is likely to meet the thrust requirements of the LOSSEI system is the Schuebeler Technologies DS-215-DIA HST EDF, which has a maximum thrust of 250 N at a mass of 3.4 kg. The maximum thrust of this EDF is also shown in Figure 4.

The estimation of the thrust that this EDF can provide underwater is based on blade element momentum theory, which follows experimental data for air-designed propellers when operated underwater [6]. A propeller can produce approximately 30 times more thrust in water than air and subsequently requires 30 times more torque at a given RPM. Therefore, the maximum thrust in the air can be matched underwater at a lower RPM. Furthermore, hall effect sensors allow a brushless motor to deliver high torque at a low RPM as the speed controller no longer relies on back electromotive force (EMF).

4. Compressible and Tensile Materials

Carbon fibre's lightweight and tensile properties have been researched and exploited for some time [27]. However, for a seaplane to submerge it requires lightweight compression strength. The material chosen is syntactic foam, in particular, a trademark Isofloat™ foam, as it is used in sea vehicles [28].

The LOSSEI's structural geometry is shown in Figure 5 and was modelled in Abaqus software. The overall structure mass, including the batteries and engine, is 57 kg (weight of 559.17 N), with the centre of gravity (CoG) located 576 mm from the nose. The mass of the empty structure is 39 kg (weight of 382.6 N). The centre of buoyancy (CoB when submerged) is 708 mm from the nose, behind the CoG.

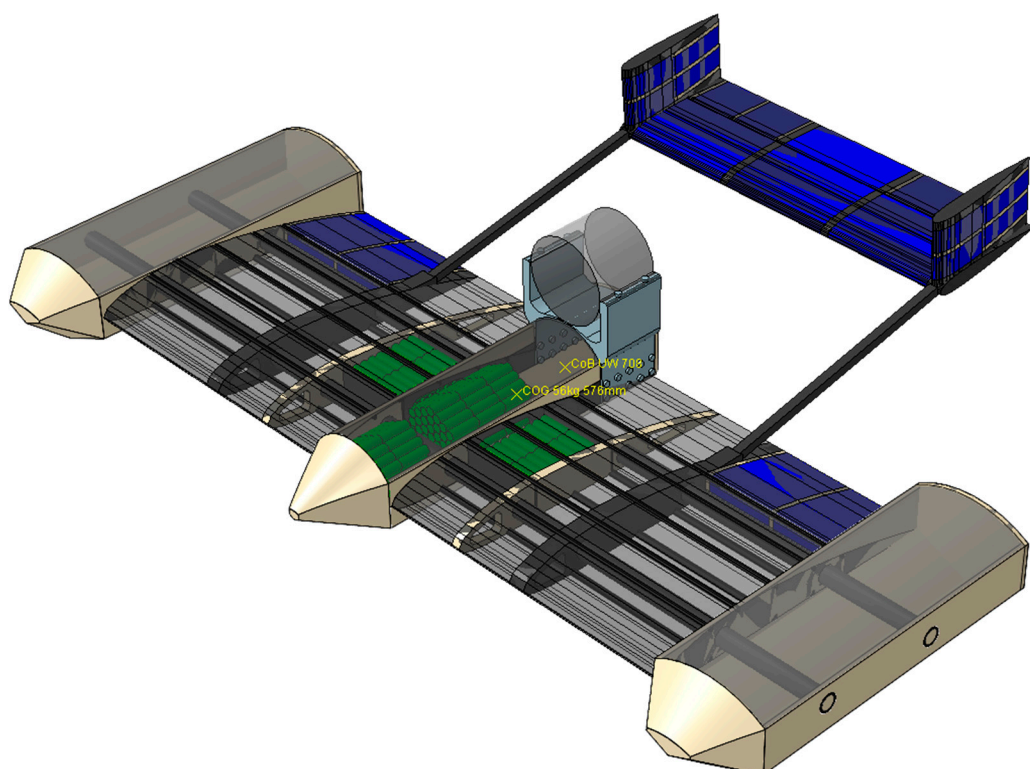


Figure 5. Wing material design considerations (**upper**) and CFD of underwater cruise condition showing pressure contours (**lower**).

The wing structure is a critical assembly that will undergo both hydrostatic and aerodynamic loads, during the operation of the craft. The wing structure is designed for aerodynamic loading; however, it is designed to be filled with water whilst submerged to avoid being crushed underwater. The syntactic foam (yellow/tan) is present in areas where the structure will experience relatively low tensile loads, but must withstand hydrostatic loads, such as the internal rib section of the wing. This is effective because the materials' low density means that the rib could be up to three times as thick as a carbon fibre rib of the same weight.

In addition, the use of syntactic foam will allow for buoyancy to be generated at that point in the wing and provide an additional surface area to interface with the spars, stringers, and wing skin that will be bonded to it. The carbon fibre (black), considered quasi-isentropic, is present in areas that will experience torsion and bending loads that will be experienced in flight, such as solid carbon fibre ribs in the wings and tails. Isofloat™ syntactic foam (yellow) is used on pressure vessels and points where pressure is applied through slamming during landing. Polyurethane (dark blue) foam is used as a very low-density filler foam to assist in withstanding the crushing loads in structures not

designed to fill up with water, or act as a pressure vessel. Anodised aluminium (light blue) is used on the engine mount to secure the main engine to the structure.

The structural design underwent a finite element analysis of all the major components, using the major known design load cases. An example of this analysis for the demi-hulls is given in Figure 6. While the structural design has yet to achieve the target weight, the early estimates show promise that refinement is likely viable. One prospect to reduce the weight is to examine composite structures of carbon fibre within a syntactic foam base. No research could be found on such composites, likely because prior to such HUAV conceptualisation, the dual demands of high compression forces when submerged, and high tensile loads when flying have not been needed.

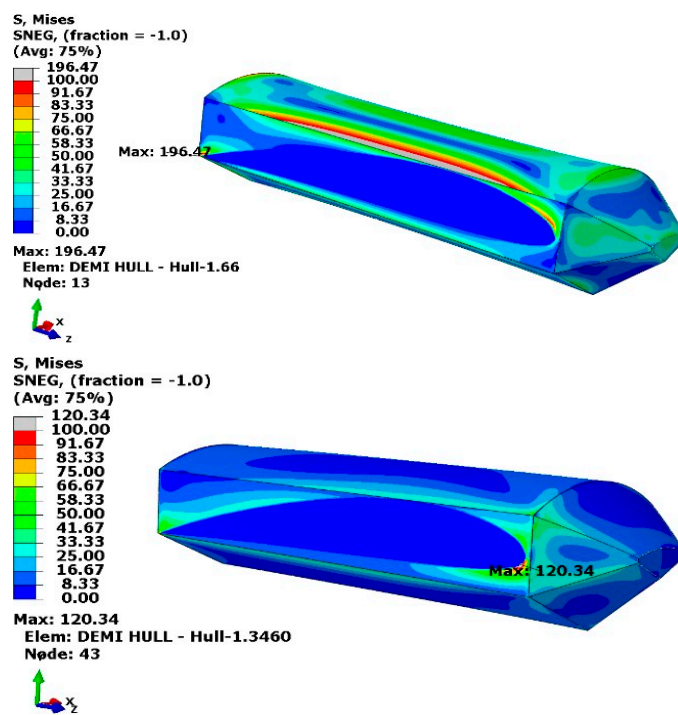


Figure 6. Demi-hull under hydrostatic pressure 710 kPa (top) and under slamming load 106 kPa (bottom).

5. Battery and Solar Recharge

The battery system for the LOSSEI is intended to comprise lithium-ion (li-ion) 21,700 cells, as shown in Figure 5 (upper) in green. Other cell options, such as NiMH hydride, were also considered for fire safety; however, NiMH's significant power draw during take off is insufficient. The Li-ion battery is split into four sections, each with a battery management system to reduce the chances of thermal runaway. The separation of the battery segments also assists in preventing chain failure, as one failed section is less likely to cause thermal runaway in the entire battery due to being separated by the syntactic foam. The nose and centre fuselage sections are located within the fuselage pressure vessel.

The wing sections will be waterproofed by a vacuum-sealed bag, filling any remaining air gaps with oil to prevent water ingress. This method is like that of conventional autonomous submarine battery packs. The total mass and capacity of the LOSSEI's battery pack, using average li-ion 21,700 cells, is estimated to be 18 kg (weight of 177 N) and 99 Ah, respectively.

This battery pack will deliver 425 A to the EDF, with a maximum current draw of 280 A. The battery system will be supplemented by solar augmentation. The fitment of thin silica-backed mono-crystalline cells (TSBMC) as solar panels on the wings allows for recharging the battery system while not in flight, increasing the operational endurance of the craft. Our research includes a 2020 study on the effectiveness of solar augmentation

in the RQ-20 Puma UAV, finding endurance could be boosted by up to 65 to 90 percent. An example solar power analysis for the LOSSEI is shown in Figure 7 to illustrate the importance the recharge offers to adapt missions.

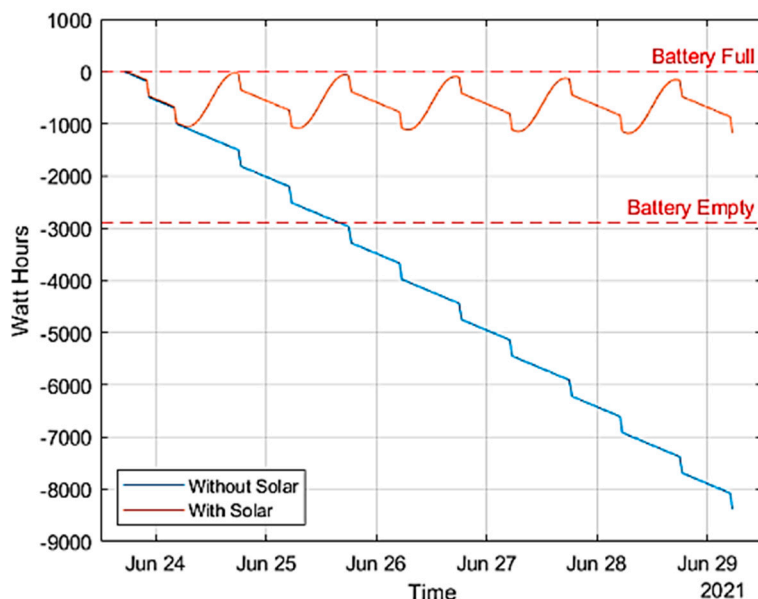


Figure 7. Example solar augmentation mission analysis from 24th June to 29th June 2021.

6. Computational Fluid Dynamics

CFD is a powerful numerical tool that is capable of simulating and performing model and full-scale optimisations in the field of ship hydrodynamics and WIG craft aerodynamics. CFD is faster and cheaper for calculating the detailed flow-field, hydrodynamic, and aerodynamic characteristics of novel craft designs in the conceptual design phase than measuring the same characteristics using scaled model tests. However, high quality experimental data are needed to validate the computed results [29,30]. According to ITTC 2011 [31], CFD could achieve a wider use if the accuracy of results, grid generation, turnaround time, and complexity of CFD could be improved.

Different CFD techniques are employed to solve complex two-phase flow problems, including the incompressible SPH formulation, which is a procedure similar to the moving particle, semi-implicit method (MPS) proposed by Koshizuka et al. [32]. The primary feature is the application of a semi-implicit integration scheme to particle-discretized equations for the incompressible flow problem, and further details can be found at [33–36].

However, this study employed the unsteady Reynolds-averaged Navier-Stokes (URANS) equations with shear stress transport (SST) $k-\omega$ physics models to represent the turbulent flow in the simulation. The use of the finite-volume URANS coupled with the SST $k-\omega$ technique in the commercial STAR-CCM+ code was based on the authors' previous experiences when compared with the results of the past SPH method in solving a relevant slam problem [37].

The design advantage of CFD in both air and underwater and transition has already been illustrated in Figures 3 and 4 for WIG effect and take-off, respectively. The 2020 version of the LOSSEI was used in wind tunnel testing, as shown in Figure 8, to validate the landing loads CFD analysis. This validation was then used as a basis for each CFD analysis, including as a basis to compare the LOSSEI's underwater cruise case. The verification of these models involved careful mesh independence and time variance techniques in each instance, and this process is illustrated later for one CFD example.

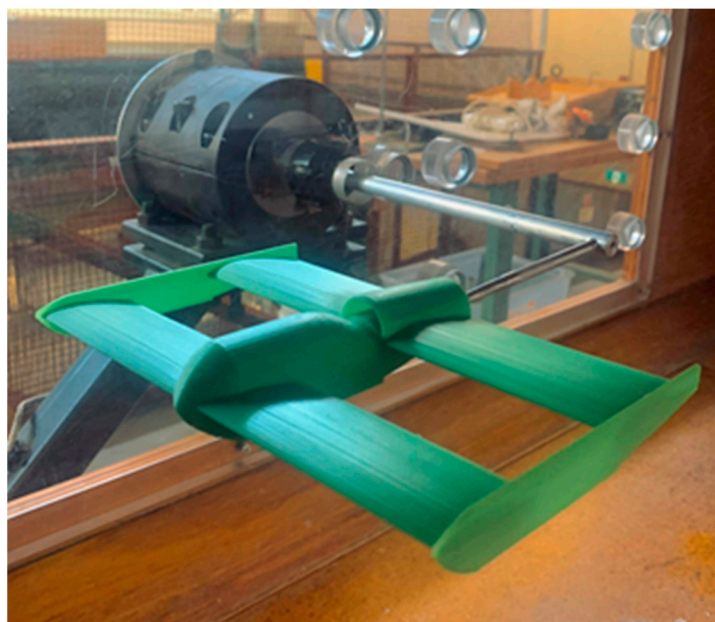


Figure 8. Wing tunnel validation testing of the 2020 LOSSEI design.

Take-off Analysis. The take-off case (Figure 4) involved a balance of the hydrodynamic, aerodynamic, and buoyancy forces to determine the vertical position of the craft in the water. The take-off case can be validated by calculating the individual forces and comparing the height above the waterline. The CFD work on WIG effect (Figure 3) was used for the aerodynamic lift, and the hydrostatic lift was calculated using volume data provided via the CAD model. The hydrodynamic lift required more detailed calculations from [38], which investigates the lift on planing surfaces for various deadrise angles.

The volume submerged as well as the area of the planing surface was found by using the same centreline height above the waterline as was found in the simulation. For example, for snapshot 5 (Figure 3) only the ends of the demi-hulls are under the water surface, with the end of the fuselage floating just above. This yielded a hydrostatic force of 1.08 N and a lift coefficient due to the planing hull angle of 0.04218 [39], leading to a hydrodynamic force of 99.8 N. From the WIG effect analysis, the lift coefficient for the aerodynamic component is 1.161, resulting in a total lift of 156.8 N. Summing these values gives 257.7 N, which is only 7 N less than the weight of the LOSSEI, indicating that the simulation provides realistic results. At this velocity, changes in the height of one millimetre can result in changes of up to 10 N in the hydrodynamic lift as the density of water is much greater than air.

The mesh for the take-off simulation was constructed with multiple key bodies to refine the critical areas of interest. The background region was the least refined, extending 10 m in front of the craft and 18 m behind. This allowed for a well-developed incoming flow and a sufficient area behind to see the wake patterns develop. The LOSSEI body itself was cut in half longitudinally to save simulation time, and its surface was refined to 6.25 per cent of the base mesh size. Additional bodies were added, such as regions focusing on the bow, front of the demi-hulls, various wake boxes, and water surface regions. These bodies were repeated three times, increasing in domain size and cell size as they moved away from the LOSSEI's body. This allowed for increased detail in the key areas, without increasing the simulation time. Ultimately, a mesh size of 430,000 and a Courant number of 0.48 were used across all six analysis points.

All the simulations were allowed to oscillate up to four times. The average lift, drag, and translation were obtained after the initial spike of lift and drag, where flow is still being established. This was conducted as opposed to allowing the oscillation to stabilise, as four oscillations allowed the flow to fully develop as well as the development of the wake

pattern. This method resulted in the lift values being within 0.3 per cent of the weight of the craft. The CFD pressure plot for snapshot 1 (3 m/s) is shown in Figure 9.

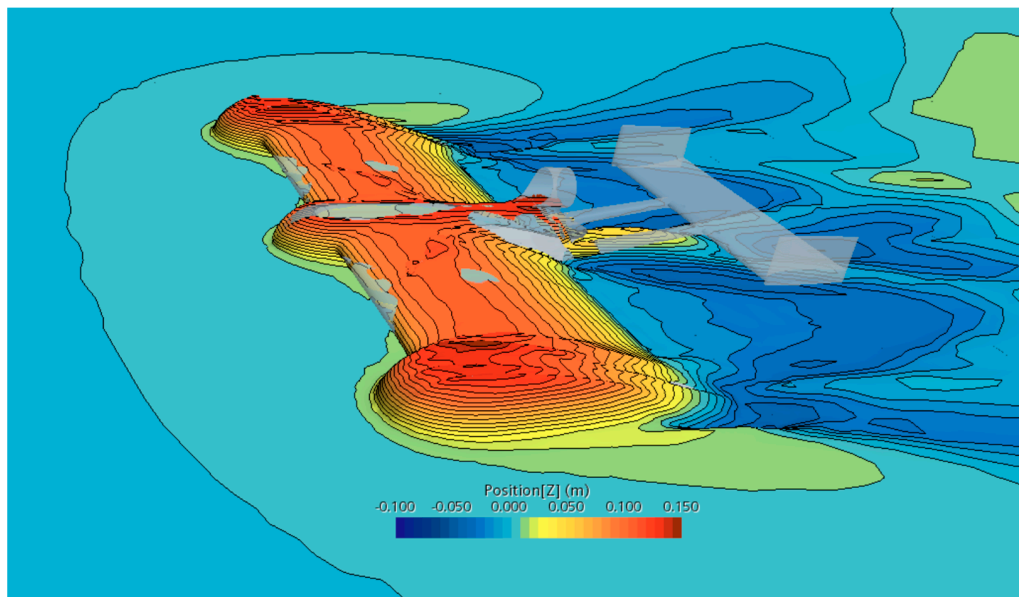


Figure 9. CFD pressure plot for take-off snapshot 1, zero-degree pitch, at 3 m/s.

Landing Loads. The team also ran a simulation to determine the landing loads of both the 2020 (Figure 8) and 2021 variants of the LOSSEI. The mesh for the landing simulation used was an overset mesh, for the movement of the craft. This overset mesh served as an intermediary mesh size between the high-resolution mesh on the craft and the lower-resolution background region. The key bodies added to refine and smooth the mesh transitions were the overlap region and the splash zone on the water surface to refine any splashes produced during the impact. Additional bodies were also placed on the water's surface, in the same fashion as the take-off simulation. The mesh and time independence studies led to a mesh optimum of 440,000 mesh and a Courant number of 0.416, allowing the simulation to depict the relationship between water and air accurately.

Data from this simulation were then used in the structural analysis of the craft. The final simulation was run for 100 ms, as this time period contains the peak forces on the three key bodies: demi-hulls, fuselage, and wings. The forces on each of these components were plotted along with the body velocity and can be seen in Figure 10.

Despite the majority of the impact acting on the demi-hulls, a large impact force can be seen acting on the wings, having the effect of causing a moment on the demi-hulls. This is conveyed on the plot as a negative force on the demi-hulls, at the time of the peak force on the wings. This spike in force is from the water jets that are generated by the deadrise angle.

Underwater Cruise. Submerging and achieving neutral buoyancy at depth requires the craft to flood the demi-hulls and wing sections that do not store equipment. The viability of the underwater cruise was explored with a CFD analysis.

The domain for the model utilised a symmetry plane to halve the computational requirement and was 9.5 m long, 4.2 m high, and 4 m wide. The mesh generated used a trimmed cell and prism layer mesh, resulting in a computational volume mesh of 372,364 cells. The simulations utilised the Reynolds-averaged Navier–Stokes (RANS) equations, with shear stress transport (SST) k-Omega physics models to represent the turbulent flow in the simulation. The liquid model was selected as the working fluid, with the density set to freshwater (997.561 kg/m^3). This density was used in all the underwater simulations, as it is lower than saltwater (1005 kg/m^3). This allows for the possibility of

the LOSSEI design to be used in fresh water and provides a safety factor to ensure there is enough buoyancy for the LOSSEI to float in seawater.

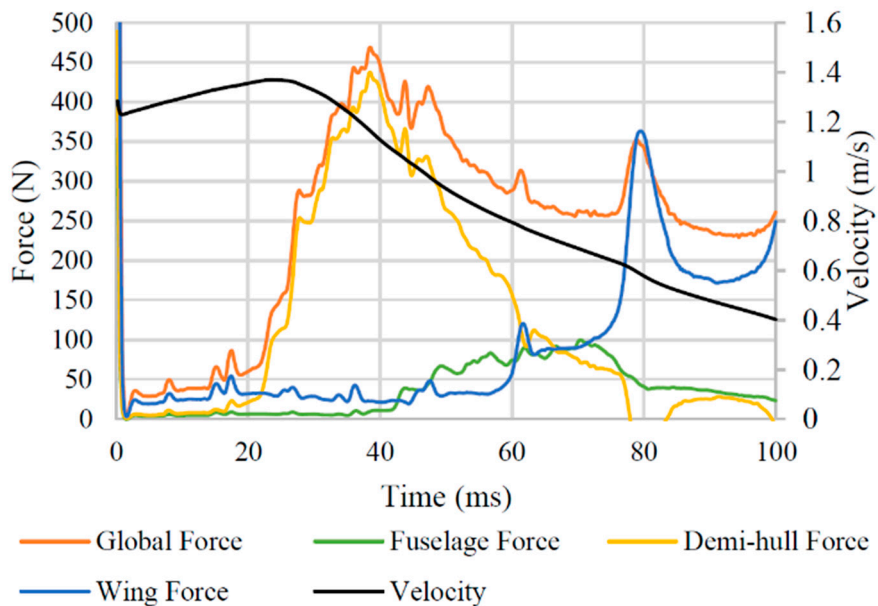


Figure 10. Impact forces on key LOSSEI bodies, compared to the overall body velocity.

A validation of the subsea CFD analysis was conducted against the in-air freestream CFD modelling. For the validation comparison to air, the working fluid was selected as gas (air) with a density of 1.18415 kg/m^3 . This comparison found that the lift and drag coefficients are almost identical for underwater and free-stream air simulations.

The mesh independence study found that the coefficients of drag and lift start to converge at a volume mesh size of 372,364 cells. Using this mesh size, the time independence study was conducted, resulting in convergence at a time step of 0.0006 s. With a velocity of 5.0 m/s and a minimum mesh size of 0.0025 m, this timestep resulted in a Courant number of 1.2.

The pressure contours are shown in Figure 11, with the maximum endurance speed estimated at 0.99 m/s or 1.92 kts. The underwater stall speed in this analysis was 0.71 m/s or 1.38 knots, and the speed of the best range was 1.20 m/s or 2.33 knots. This analysis also estimated the subsurface energy and thrust requirements for the best underwater endurance, giving the total drag for the LOSSEI as 33.64 N. The drag force is substantially less than that of the selected EDF, at least when operating in the air.

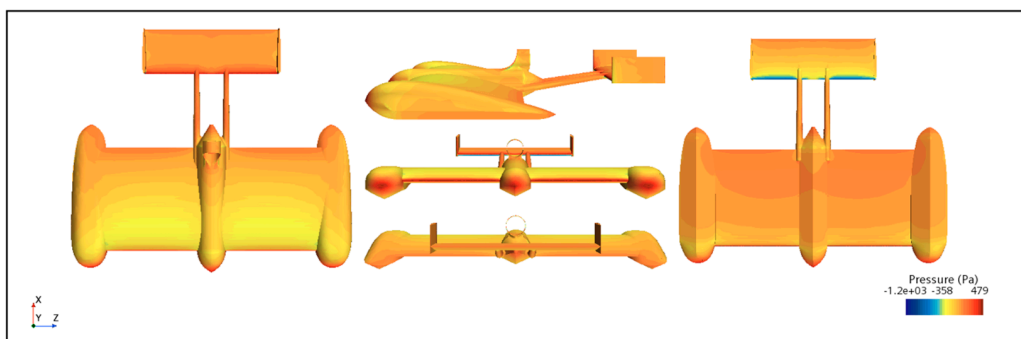


Figure 11. Pressure contours of the underwater cruise condition.

Surfacing. A surfacing simulation was conducted to check the dynamic effect of buoyancy from depth to the surface and the associated pressure and thus, the structural forces. The main differences from the underwater cruise were the inclusion of an overset (Chimera) mesh, six degrees of freedom (DOF) solver, and a volume of fluid (VOF) model to simulate the water's surface. The base RANS and SST k-Omega models remained the same as before, and the mesh was generated using trimmed cell and prism layer mesh.

The total fluid domain was 22.0 m in length, 14.0 m in width, and 22.0 m in height. This length allowed enough distance in front of the craft to generate the water's surface accurately and enough behind the vessel not to disturb the wake.

The width of the tank was considerably wider than that of the underwater simulations, as a symmetry transformation was unable to be used as that would affect the accuracy of the DOF solver; therefore, that whole geometry had to be modelled. The height was set at 17.0 m below and 5.0 m above the water's surface. This allows adequate fluid below the craft, initially set at 10.0 m below the water's surface.

The overset mesh domain was a 3.0 m by 4.0 m by 2.5 m rectangle encompassing the LOSSEI geometry. For this set of simulations, the LOSSEI body's motion is most important to the analysis, so overset meshing and DFBI solvers are crucial inclusions. The parameter for this simulation was the maximum pitch angle of the LOSSEI as it ascends to the surface.

The mesh independence results, Figure 12, show that the volume mesh sizes of 593,269 cells and 1,405,796 cells yielded the most similar pitch angles. Therefore, the volume mesh with the lower cell density was selected to save computational time (2.6 h compared to 4.5 h). The time independence study was then conducted with the selected volume mesh. The results showed minimal change between the timesteps of 0.02 s and 0.005 s (0.6 deg). Due to this minimal change, the timestep of 0.015 was selected, resulting in a Courant number of 1.0. Unfortunately, when the current velocity was increased to test the relationship between the water current and the LOSSEI's ascent, the time step had to be reduced to 0.0075 s. This timestep provided a Courant number of less than 1.0 for all the tested velocities, obtaining more stable results.

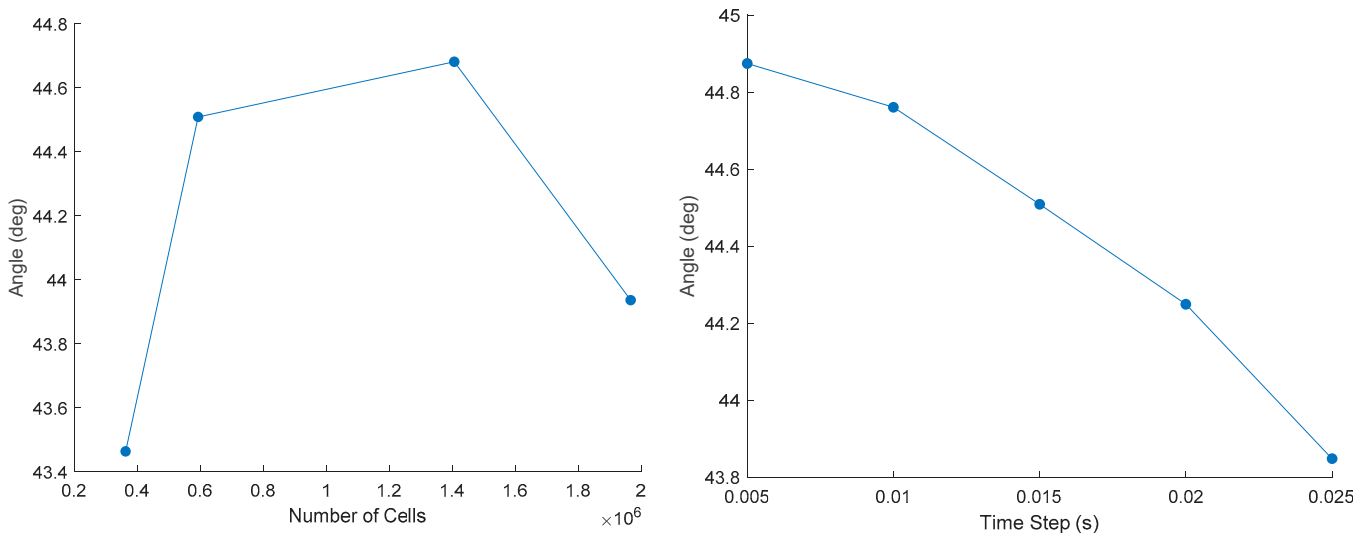


Figure 12. Mesh independence and time independence studies for the CFD of the underwater surfacing study.

A Eulerian multiphase interaction had to be set up, in conjunction with the VOF of a flat wave to generate the water's surface accurately. The phases of the Eulerian multiphase interaction were set as water (density 997.561 kg/m^3) and air (density 1.18415 kg/m^3). The VOF was selected as a flat wave, as the interaction of the LOSSEI breaching the water's surface, at this stage, was not required to have waves set. The current (water) and the wind (air) velocities were set within the VOF wave function.

The LOSSEI was set at 10 m below the water's surface, with no additional current speed or body motion for these simulations. The DFBI model was set to Z-motion to record the vertical position of the craft and Y-rotation to record the pitch. After 0.05 s of physical run time, the DBFI model was released, and motion was allowed. This provides enough time for the fluid flow to fully develop, which would minimise any disturbance at the beginning of the simulation.

The results in Figure 13 show that as the vessel gradually rose towards the surface, the pitch angle increased to approximately 44-degrees. At this point, the pitch remained constant, until the LOSSEI reached the water's surface. At the surface, the nose began to pitch down until it reached rest. The time taken for the LOSSEI to reach the water's surface was recorded to be 9.21 s from release, which shows that the average velocity over 10 m is equivalent to 1.09 m/s.

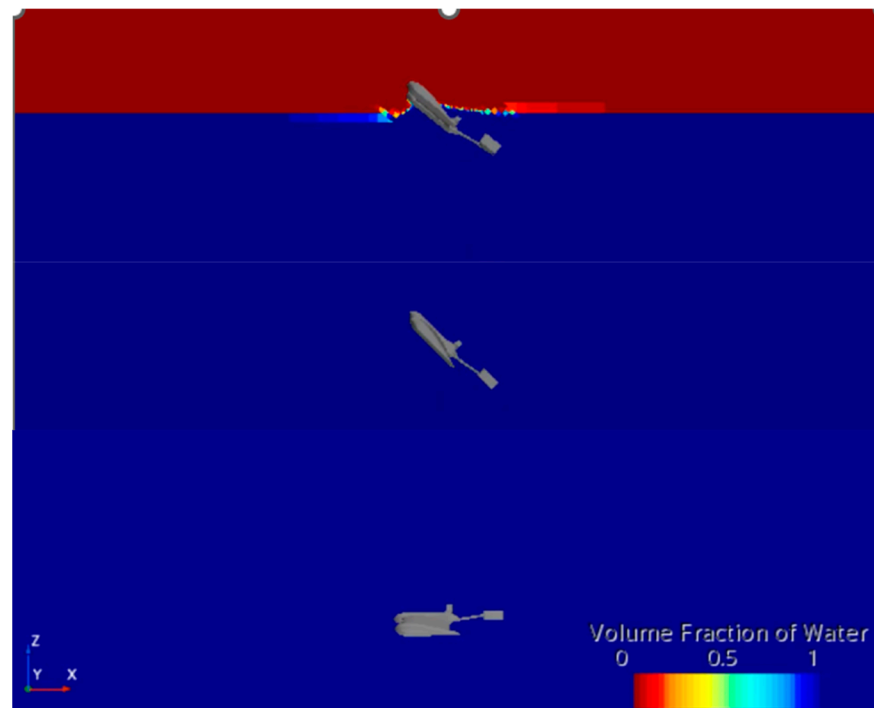


Figure 13. Concatenation of the CFD simulation of surfacing.

WIG in Rough Seas. It is rare that the surface of a sea where the LOSSEI will be operating will be perfectly smooth, and so, the effect of waves on lift and drag must be accounted for. Research in [26] examined the effect of waves on the WIG effect for an NACA4412 airfoil, modelling the waves as a sinusoidal motion with an amplitude of 0.05 for the wing chord (c) and a wavelength of $5c$. It was found that as the airfoil moved over the waves, the lift coefficient would oscillate with the same period as of the passing waves. This is due to the change in instantaneous h/c over the period of the waves. When the periodic average was taken for the lift coefficient, it was approximately equal to the lift coefficient of the same height-to-chord ratio but without the waves. For a given height-to-chord ratio, the amplitude of these oscillations became more pronounced with increased angles of attack but remained approximately constant relative to their time-averaged lift coefficient. The relative amplitude of the oscillations of the moment coefficient was smallest at low angles of attack and peaked at a 14-degrees angle of attack. Therefore, it is best to fly at an angle of attack between 2 and 10° to minimise these fluctuations. The effect of waves on the LOSSEI WIG effect was analysed numerically, following this research approach [26].

The wavy seas simulations included a Eulerian multiphase volume of fluid (VOF) model with gravity. To accurately model the craft's movement over the waves, the fifth-order wave type was selected. Although flight over only a basic sinusoidal wave was

required for the purposes of this research, and the first-order wave model would have been sufficient, the fifth-order wave model included an additional velocity parameter. This allowed the geometry to be set as the reference frame and airspeed to be set as the additional velocity, whereas using the first-order wave model would have required the craft to be translated along the x-axis with a dynamic fluid body interaction (DFBI) motion and an overset and background mesh. The fifth-order waves model also has greater flexibility in testing unique cases, such as shallow water waves or where there are large discrepancies between the velocity of the waves and the free-stream air.

The mesh contained a heavily refined region at the free surface. STAR-CCM+ guidelines recommend using an anisotropic mesh to accurately simulate fifth-order waves, with the X and Y domain sizes as 1/80th of the wavelength and the Z domain size as 1/20th of the wave height. These absolute values are manually changed for each test case, based on the wave profile being used in that simulation. The geometry had surface refinements and wake refinements.

The simulations were run using the Reynolds-averaged Navier–Stokes (RANS) equations, for a segregated unsteady flow. The RANS model was used as it provides adequate accuracy in modelling turbulence, is very stable for incompressible flows, and is computationally efficient. The K- ω shear stress transport (SST) was used to model the turbulence.

The verification of the wavy seas simulations was completed through a mesh independence study and a time independence study, using the peak lift coefficient. The mesh that was decided on for use in the final set of simulations contained 1140 k cells, with a Courant number of 0.7 with a difference of 0.1 per cent from the smallest Courant number tested. As the simulation progressed, the peak lift coefficient changed slightly over each wave but converged to a steady value the longer the simulation ran. The second wave reliably generated a peak lift coefficient of around 0.1 per cent absolute of the converged value. For this reason, and to keep computation time to a minimum, all the results were taken from the second wave. Using the aforementioned parameters provided computation times between 10 and 18 h, dependent on the specific wavelength being tested.

For the wavy sea simulations, both the height-to-chord (h/c) and wave height-to-chord (w/c) were changed. The wave height was a function of the ride height given by Equation (1), which provides a 0.1 chord length clearance between the wave's peak and the bottom of the demi-hulls. Thus, the minimum test condition was a 0.3 height-to-chord, corresponding to a wave height of 0.2. Note the height-to-chord is measured from the average height of the wave, halfway between the peak and the trough:

$$\frac{w}{c} = 2 \left(\frac{h}{c} - 0.2 \right) \quad (1)$$

As the craft flew over the waves, the lift, drag, and moment were all found to fluctuate as the height-to-chord periodically became smaller and larger. The general trend in all of the tests was that the larger the waves, the larger these fluctuations, and as the clearance above the waves increased, the magnitude of the fluctuations decreased. All the tests of wavy seas were completed for a zero degree pitch angle only; it is the assumed flight condition for all comparisons and calculations. The variation in the lift coefficient is shown in Figure 14, where the largest fluctuations over the largest waves modelled was the high lift coefficient being 2.4 times the lowest lift coefficient. The trends in the fluctuations of the drag coefficient were like that of the lift coefficient; however, the points of lowest drag were when the lift was highest and vice versa. Unlike the results for lift, the most extreme fluctuation in drag was the 0.6 wave height-to-chord flight condition as opposed to the 1.0 wave height-to-chord flight condition for lift fluctuation.

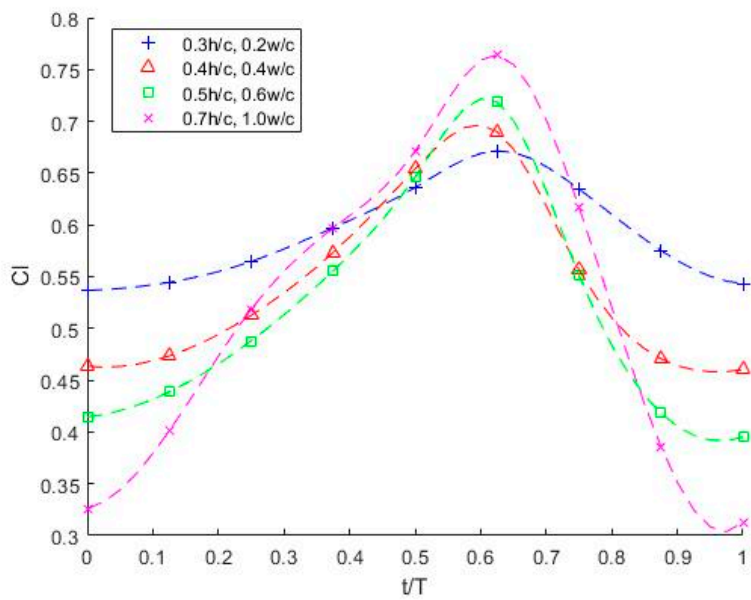


Figure 14. Fluctuations in lift coefficient with changing height-to-chord and wave-to-chord ratios, against the non-dimensionalised time (t) flying over a wave of period (T).

Most important to the craft's stability is the fluctuations of the moment coefficient over wavy seas, as shown in Figure 15. Consistent with [26], the larger the wave height was, the greater the fluctuations were. In the most extreme case, the moment coefficient at the peak was twice what it was at the low point. The moment coefficient was always positive, meaning that the craft wanted to pitch up; however, this was due to an unfortunate excess tail-set angle in this design iteration of four degrees nose-down instead of about one degree nose-up.

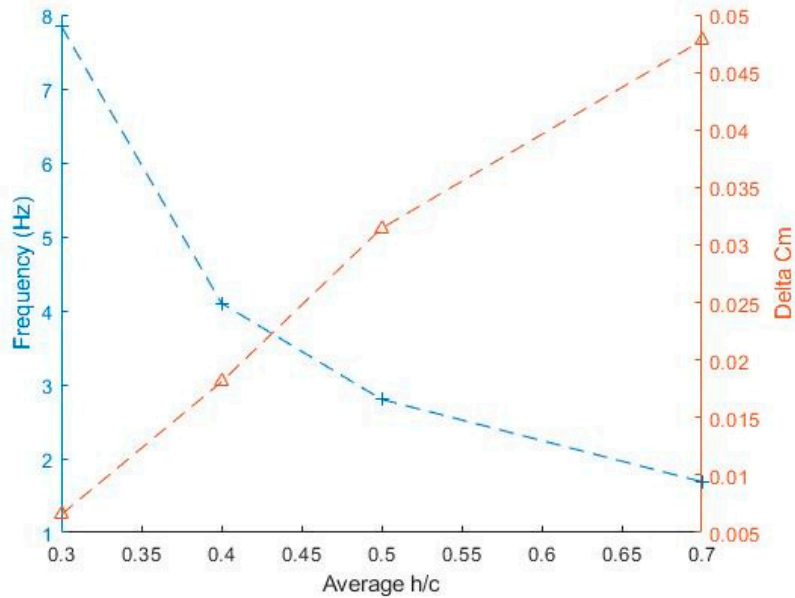


Figure 15. Frequency and magnitude of fluctuations in moment coefficient over waves as a function of the height-to-chord (aircraft above ground).

7. Future Iterations

Early work and the more recent research literature highlight several changes to make to the next iteration of the LOSSEI craft. Student conceptual design work in 2022 examined

if the submersible seaplane concept can be scaled up and crewed, similar to the U.S. research in 2010 on the viability of such a craft for special forces insertion and extraction in littoral environments [40] such as with the more recent ‘flying boats’ that have allegedly been demonstrated [41]. Our recent student work on upscaling the LOSSEI also examines if the design margins made available by the new technologies make submersible seaplanes more or less viable. As such, our lessons for the LOSSEI redesign may be seminal in shaping the new HUAV class. The focus of future iterations needs to be on two broad areas, including optimization and reducing several specific risks; however, these are interrelated and the focus of some research.

WIG Stability. WIG crafts experience complex longitudinal stability, where the lifting advantage depends on the height above ground, as previously mentioned; however, that lift advantage also varies with the angle of attack. As such, there are three distinct ground effect regions [24] that present some difficulty in maintaining that optimum advantage [19], especially in the presence of waves that vary in height [42]. The simulation of the longitudinal stability problem was advanced by [43,44], including some lateral stability. A recent Chinese advancement comprises developing an H ∞ attitude controller that can accommodate the problem of the change of wave height, with advantages in lateral and directional stability [45]. However, as a caution, this research is based on a novel wind tunnel modelling of wavy ground, and further Chinese research has found that when h/c is low, there is a wind shear force that can cause the forthcoming wave crest to produce water spray with stability concerns [46]. Moreover, as we discovered, a general simulation of the craft going into and out of the ground effect is complicated by the changing lift and drag, whereas these are critical design areas to explore early. Fortunately, research by [47] has produced relationships with a good agreement and reduced computation for early WIG concept simulations.

Compound Wings and Optimised Endplates. The stability concerns at a low clearance and the prevalence of waves mean a WIG craft for open ocean work likely needs a compromise of in-ground effect and conventional out of ground lift, usually provided by a compound wing. Students have developed such a compound wing for the up-scaled version of the LOSSEI, with a type of low aspect ratio inner WIG wing that blends to form a fuselage and a higher aspect ratio outer conventional wing. The advantage of blending the fuselage to the wing for a HUAV was also proposed by the U.S. study [40]. The transition in going outboard between the two compound wings is marked by the endplate of the WIG wing, which like the LOSSEI, is also a demi-hull for landing, take-off, and surface stability. Such a design of compound wings for a balance of WIG and conventional flight can be explored using a practical model, developed by [48], including aiding with the longitudinal stability by the longitudinal bias of the outer wing towards the tail. Another aspect that needs optimization is the placement of the endplates or demi-hulls, which for the LOSSEI case was as outboard as possible to maximise the spanwise WIG effect. Moving to a compound wing means a trade-off. The effects of the endplates were researched by [49], and while these were confirmed to be positive for lift and drag, they also harmed height stability.

Take-off Case. Another difficulty we experienced was in generating the take-off case in which there are complex hydrodynamic, aerodynamic, and buoyancy forces. As described earlier, this is a critical case for sizing the engine and battery electrical loading, determining the wing set angle, and for empennage placement; therefore, it needs to be accurate. We examined a set number of solutions and interpolated them. The research by [50] develops a solution approach and multi-objective optimization for a WIG take-off case, including a catamaran hull and compound wing. Such an approach offers improved accuracy for this critical design case.

Water Entry, Exit, and Endurance. The LOSSEI design uses a seaplane take-off and landing approach with flooding and buoyancy systems to submerge or exit the water, similar to research by [51]. The new Chinese HUAV, known as Nezha III, also appears to use a surface landing and take-off transition, albeit a vertical take-off [11,14]. The Nezha III has ‘tradeoffs between hydrodynamic and aerodynamic performance’ that the LOSSEI did

not explore, instead favouring aerodynamics and checking the effects hydrodynamically. Such trade-offs are worth exploring to improve underwater endurance. Chinese research has also explored dynamic and CFD modelling for direct entry approaches [7,8] and more recently, a dynamic water exit [13] to '*rapidly exit from water with a wide range of pitch angles*', for better survivability in bad sea states. We explored structural forces with a conventional surface landing and found them to be the highest design case and a major driver of structural weight estimates. Ideally, the LOSSEI needs extendable and retractable demi-hulls to increase clearance during the landing impact, which in turn contributes to drag. Dynamic water entry and exit would be structurally limiting for conventional aircraft shapes.

Signature. Every effort has been made to limit the LOSSEI signature to maritime high-frequency radars (i.e., HFSWR and OTHR [17]) and infrared satellites. Examples include its relatively low speed, no propellers, composite structures, and ocean proximity. Methods to analyse radar signatures before proof-of-concept prototyping have been limited [39] but improving, such as [52,53], although nothing specific to the frequencies of fixed strategic assets. According to [39], tailoring the aircraft shape is the most effective strategy for signature reduction; however, this approach is unlikely to be possible given the tension already between sensitive hydrodynamics and aerodynamics. Radar absorbent material will likely add too much weight for the LOSSEI, unless applied only to key zones as proposed by [54], although such materials are highly susceptible to saltwater corrosion [55].

Buoyancy. The LOSSEI design envisages a buoyancy engine to help control the subsea depth and aims to prepare for diving by flooding the wings and demi-hulls with batteries, sealed as outlined earlier. The Nezha III HUAV design also floods the wings. It has also tested such a buoyancy engine, described as a 'lightweight super high-pressure pneumatic buoyance control' that embraces the buoyancy–pitch coupling of its underwater gliding (UG) [11]. Such an implementation of a buoyancy engine reportedly increased the depth of the Nezha variants from 5 m to 50 m, an encouraging system maturity for the LOSSEI. According to Nezha's designers, 'The only driving force pushing a UG forward is the horizontal component of lift induced by the gliding motion due to the inequality between gravity and buoyancy.' Further, 'Without any propulsion, gliding motion is quite energy efficient.' Exploiting underwater gliding subsea is similar to the WIG effect, exploited for greater endurance above the sea. A review this year in [44] explains the propulsive concept of such underwater gliding:

"On ingesting water, it becomes negatively buoyant and starts to sink, developing a download component of force. With wings attached to its body, the vehicle can develop lift and drag force in the horizontal plane. This resultantly develops a forward motion. Upon reaching a certain depth, water is expelled making the vehicle positively buoyant and thus causing it to float. The wing-lift again produces a forward motion, and this cycle is repeated. The profile traced by the glider is saw-tooth in shape". (p. 05000-2)

This review covers approximately 50 prototyped glider designs [56]. It concludes that 'The underwater glider is a budding technology that is still in its infant stage' and that 'An efficient buoyancy engine is an integral part of an underwater glider as it helps in achieving higher depth along with more range of travel.' Future LOSSEI iterations should explore if such gliding is viable combined with the EDF propulsion to extend the submerged travel endurance. The CFD analysis has provided the basic lift and drag profiling to enable simulation and steering, like in [57] and what hydrodynamic refinements may be necessary similar to [58]. We acknowledge there may be trade-offs to be made to the aerodynamics, given the precedents thus far.

Weight. The LOSSEI's estimated weight from the structural analysis was around 100 per cent heavier than the target weight, primarily driven by the significant deceleration loads upon water landing (impact). A significant factor in the size of these loads is the main fuselage and demi-hull distances below the wing, as this margin 'cushions' the impact. The distance is kept small, at around 70 mm to facilitate a desirable WIG effect (i.e., h/c

around 0.2), with a margin for the hulls above the water (i.e., wings at 140 mm above the water is $h/c = 0.2$, with hull bottoms at 70 mm above the water). Future iterations of the LOSSEI will need an extendable and retractable set of demi-hulls, of at least twice the current below-wing clearance (i.e., extending another 70 mm). This extension and retraction could be achieved with a rotating arm on the main spar, so the demi-hulls are 70 mm aft when retracted and 70 mm forward when extended, as this would increase the stability of landing through a greater longitudinal flying static margin and provide an option to move the centre of gravity and centre of buoyancy for underwater manoeuvre or gliding. The extension of the demi-hulls will reduce the wing impact loads and therefore reduce the structural weight.

Autonomy. The LOSSEI requires a high degree of autonomy to operate without compromising its position with datalinks. The literature suggests controllers are feasible in all mission phases; however, the mission profile is adaptive, allowing the LOSSEI to change mediums depending on the weather, threats, and mission success. Training the higher-order artificial decision making to adapt the mission to such inputs will require some generic training in navigation, threat monitoring, and weather monitoring, followed by specific training in the geospatial, meteorological, and intelligence of each mission. Such training will require human autonomy teaming with responsible commanders and operators to build the necessary trust to safely deploy and recover the LOSSEI on autonomous missions [59].

8. Validation

Our HUAV design needs validation, like that documented in 2021–22 on the designs by [11] and [14]; however, it is important to first fully explore the best return on investment, optimise the digital conceptualisation, and then do a proof-of-concept validation of the numerical simulations. Finally, the digital conceptualisation will need to be optimised again from the fully validated simulations before full prototypes are developed. In a military context, the most likely best return on investment is proposed as a recoverable sonobuoy HUAV operating from a parent maritime patrol aircraft, searching for submarines or uncrewed underwater vehicles. Such a craft would dive and breach to supply operation in diverse sea states by avoiding take-off and landing, and it would likely use reel-in and reel-out release and recovery techniques under development for parent–child aircraft combinations. Several innovations can be drawn from the LOSSEI research, concerning the use of EDF in air and water, battery power and storage, the composite use of syntactic foam and carbon fibre, and extensive optimisation through CFD analysis before a prototype.

A new risk is the impact of diving, potentially requiring folding wings, a reverse thrust, a reinforced nose cone, and dual retractable EDFs. The parent–child relationship offers recharging, superior sensor fusion and data processing, and reduces the autonomy challenge compared to the LOSSEI; however, release and recovery from parent aircraft pylons brings a new dynamic and other compatibility risks. An example validation program for such a recoverable sonobuoy HUAV, given in Figure 16, focused on the risks of impact shock, EDF operation, material strength optimisation, configuration, underwater performance, and parent–child aircraft compatibility. Our intent here is not to cover another conceptual design, rather to legitimately explain why our LOSSEI design has to evolve to ‘market forces’ and why design validation will require additional funding and a structured approach to such investment.

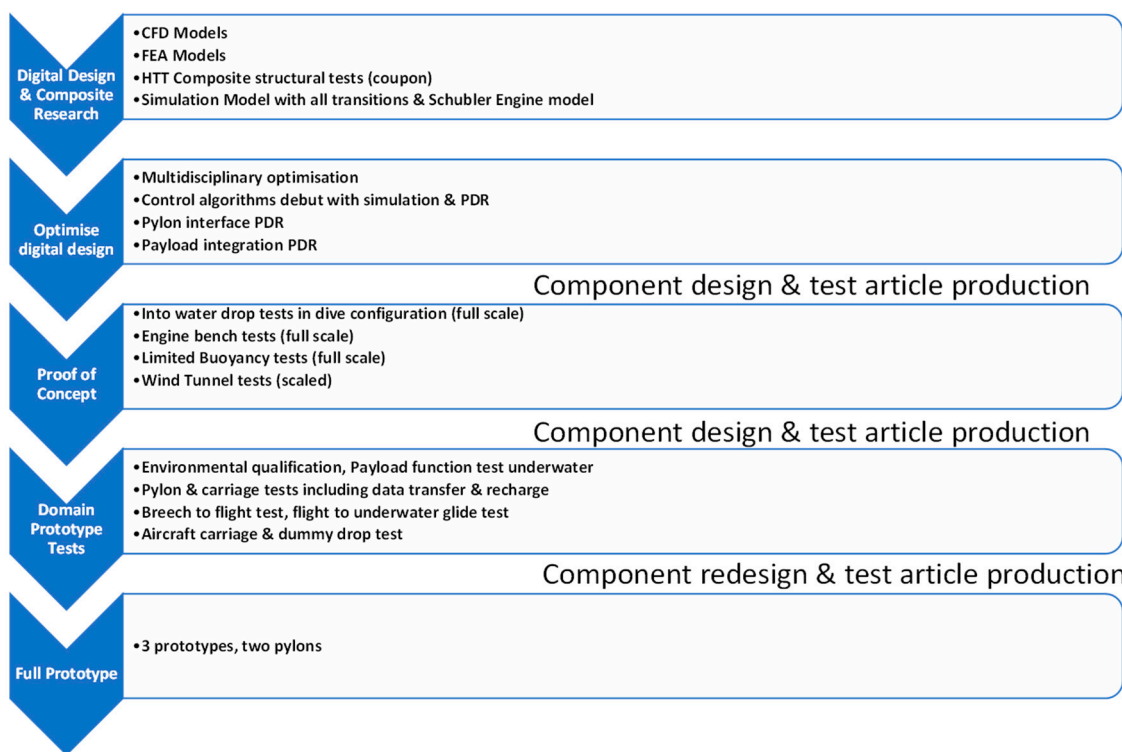


Figure 16. Example validation proof-of-concept prototyping proposal for a child HUAV operating from, and back to, a parent aircraft. Note the timeframes from top to bottom have been removed. HTT is high throughput testing.

9. Conclusions

A submersible seaplane or HUAV, known as the LOSSEI has been conceptually designed by staff members from Australian and Egyptian universities that exploits developments across five key technologies to achieve viability. First, using the wing-in-ground effect has substantially improved flight endurance, reduced the power required, and likely reduced detection compared to the flight out of ground effect. Second, new electric ducted fan designs offer sufficient propulsion for take-off and cruise while enabling limited underwater travel to aid insertion and recovery. Third, merging carbon fibre from aircraft with syntactic foam from undersea vessels strengthens both domains. Fourth, the development of Lithium-Ion batteries provides sufficient power to take off and perform missions. At the same time, conformal solar technology allows the batteries to recharge while on listening stations during the day. Finally, advances in CFD enable designers to examine craft design features in air, water, and across the transitions.

There are numerous recent developments in HUAV craft, particularly by Chinese researchers in the last two years, that inform this conceptual design and its future proof-of-concept prototype testing. Important developments have occurred that likely advantage the LOSSEI conceptual design, concerning compound wing and endplate optimization, buoyancy engines, underwater gliding simulation and control, WIG stability controllers and simulation, and aircraft signature modelling. These developments combine with the lessons taken from this iteration for improvements, such as retractable and extendable demi-hulls to cushion the landing impact better and reduce weight.

Subject to another conceptual design iteration, the LOSSEI concept is ready for proof-of-concept prototype testing to validate the numerical simulations and the assumptions concerning new composite materials, EDF propulsion, and autonomy. Given the seminal nature of HUAV design and research and some of the unique innovations proposed, the lessons learned from this iteration will likely be significant to other designers and researchers. Based on customer feedback, our research team has adjusted our HUAV design

research work to look at a better return on investment, shifting to the design of a recoverable sonobuoy HUAV operating from a maritime patrol aircraft. This shift in mission leverages some aspects of the LOSSEI design, which will hopefully see these research initiatives validated in the future for both HUAV mission types.

Author Contributions: Conceptualization, K.F.J. and A.A.S.; methodology, K.F.J. and A.A.S.; software, A.A.S.; validation, K.F.J. and A.A.S.; formal analysis, K.F.J. and A.A.S.; investigation, K.F.J. and A.A.S.; resources, K.F.J. and A.A.S.; data curation, K.F.J. and A.A.S.; writing—original draft preparation, K.F.J.; writing—review and editing, K.F.J. and A.A.S.; visualization, K.F.J. and A.A.S.; supervision, K.F.J. and A.A.S.; project administration, K.F.J. and A.A.S.; funding acquisition, K.F.J. and A.A.S. All authors have read and agreed to the published version of the manuscript.

Funding: This research received no external funding.

Institutional Review Board Statement: Not applicable.

Informed Consent Statement: Not applicable.

Data Availability Statement: Data is not available.

Acknowledgments: Staff from Ron Allum Industries and Thales Underwater Systems Australia have helped supervise this research. We thank all staff and students who have worked on this conceptual design, particularly Georgina Hazenberg, Bradley Hunter, Edison Jewson, Nicholas Carroll, Angus Gebers, Adam Elgayar, David Champ, Gennady Shpak, Vraj Patel, and Evgeny Morozov.

Conflicts of Interest: The authors declare no conflict of interest.

References

- Carroll, N.J.; Champ, D.; Gebers, A.; Jewson, E.; Patel, P.; Shpak, G.; Joiner, K.F.; Swidan, A. Low-Observable Submersible Sea-plane for Electronics Intelligence (LOSSEI): A conceptual design and analysis. In Proceedings of the 2021 6th SIA Submarine Science, Technology and Engineering Conference (SubSTEC6), Adelaide, Australia, 8–10 November 2021.
- Joiner, K.F.; Swidan, A.; Jewson, E.; Carroll, N.; Champ, D.; Shpak, G. Submersible Seaplanes as the Path to Hybrid Flying and Diving Craft. In Proceedings of the ISUDEF 2021—International Symposium on Unmanned Systems and the Defense Industry 2021, Howard University, Washington, DC, USA, 26–28 October 2021.
- Hunter, B.; Swidan, A.; Joiner, K.F.; Hazenberg, G. Accurate Prediction of Landing Loads for a New Design of a Wing-in-Ground Maritime Surveillance Drone—CFD Investigation. In Proceedings of the 2021 31st International Conference on Computer Theory and Applications (ICCTA), Alexandria, Egypt, 11–13 December 2021. [[CrossRef](#)]
- Swidan, A.; Joiner, K.F.; Jewson, E.; Carroll, N.; Champ, D.; Shpak, G. A Novel Flying and Diving WIG Craft for Electronics Intel-ligence—A Conceptual Design. In Proceedings of the IEEE 2022 International Telecommunications Conference (ITC-Egypt), Alexandria, Egypt, 26–28 July 2022. [[CrossRef](#)]
- Yang, X.; Wang, T.; Liang, J.; Yao, G.; Liu, M. Survey on the novel hybrid aquatic–aerial amphibious aircraft: Aquatic unmanned aerial vehicle (AquaUAV). *Prog. Aerosp. Sci.* **2015**, *74*, 131–151. [[CrossRef](#)]
- Parth, V.S. Characterization, and Optimization of UAV Power System for Aerial and Submersible MultiMedium Multirotor Vehicle. Bachelor’s Thesis, Graduate School—New Brunswick, Rutgers, The State University of New Jersey, New Brunswick, NJ, USA, 2016.
- Xu, B.; Li, Y.; Feng, J.; Hu, J.; Qi, D.; Yang, J. Research on the water-entry attitude of a submersible aircraft. *SpringerPlus* **2016**, *5*, 1933. [[CrossRef](#)] [[PubMed](#)]
- Yang, J.; Li, Y.; Feng, J.; Hu, J.; Liu, A. Simulation and experimental research on trans-media vehicle water-entry motion characteristics at low speed. *PLoS ONE* **2017**, *12*, e0178461. [[CrossRef](#)] [[PubMed](#)]
- Wang, Q.; Wu, S.; Hong, W.; Zhuang, W.; Wei, Y. Submersible Unmanned Aerial Vehicle: Configuration Design and Analysis Based on Computational Fluid Dynamics. In *MATEC Web of Conferences*; EDP Sciences: Les Ulis, France, 2017; Volume 95, p. 7023. [[CrossRef](#)]
- Weisler, W.; Stewart, W.; Anderson, M.B.; Peters, K.J.; Gopalarathnam, A.; Bryant, M. Testing and Characterization of a Fixed Wing Cross-Domain Unmanned Vehicle Operating in Aerial and Underwater Environments. *IEEE J. Ocean. Eng. Ing.* **2018**, *43*, 969–982. [[CrossRef](#)]
- Lu, D.; Xiong, C.; Zhou, H.; Lyu, C.; Hu, R.; Yu, C.; Zeng, Z.; Lian, L. Design, fabrication, and characterization of a multi-modal hybrid aerial underwater vehicle. *Ocean Eng.* **2021**, *219*, 108324. [[CrossRef](#)]
- Wei, Z.; Teng, Y.; Meng, X.; Yao, B.; Lian, L. Lifting-principle-based design and implementation of fixed-wing un-manned aerial–underwater vehicle. *J. Field Robot.* **2022**, *39*, 694–711. [[CrossRef](#)]
- Wei, J.; Sha, Y.-B.; Hu, X.-Y.; Yao, J.-Y.; Chen, Y.-L. Aerodynamic Numerical Simulation Analysis of Water-Air Two-Phase Flow in Trans-Medium Aircraft. *Drones* **2022**, *6*, 236. [[CrossRef](#)]

14. Lyu, C.; Lu, D.; Xiong, C.; Hu, R.; Jin, Y.; Wang, J.; Zeng, Z.; Lian, L. Toward a gliding hybrid aerial underwater vehicle: Design, fabrication, and experiments. *J. Field Robot.* **2022**, *39*, 543–556. [CrossRef]
15. Zeng, Z.; Lyu, C.; Bi, Y.; Jin, Y.; Lu, D.; Lian, L. Review of hybrid aerial underwater vehicle: Cross-domain mobility and transitions control. *Ocean Eng.* **2022**, *248*, 110840. [CrossRef]
16. Bi, Y.; Jin, Y.; Lyu, C.; Zeng, Z.; Lian, L. Nezha-Mini: Design and Locomotion of a Miniature Low-Cost Hybrid Aerial Underwater Vehicle. *IEEE Robot. Autom. Lett.* **2022**, *7*, 6669–6676. [CrossRef]
17. Joiner, K.F.; Atkinson, S.R.; Castelle, K.; Bradley, J. Near-Term Asian War: Impacts and Options for Australia’s Submarine Program. In Proceedings of the 5th Submarine Science, Technology and Engineering Conference (SubSTEC5), Fremantle, Australia, 18–22 November 2019; pp. 15–28.
18. Yun, L.; Bliault, A.; Doo, J. *WIG Craft and Ekranoplan: Ground Effect Craft Technology*; Springer: Boston, MA, USA, 2010.
19. Nirooei, M. Aerodynamic and static stability characteristics of airfoils in extreme ground effect. *Proc. Inst. Mech. Eng. Part G J. Aerosp. Eng.* **2018**, *232*, 1134–1148. [CrossRef]
20. Swidan, A. A novel concept in reducing wetdeck slamming loads—CFD investigation. In *ISOPE International Ocean and Polar Engineering Conference*; ISOPE: Mountain View, CA, USA, 2019.
21. Barjasteh, M.; Zeraatgar, H.; Javaherian, M.J. An experimental study on water entry of asymmetric wedges. *Appl. Ocean Res.* **2016**, *58*, 292–304. [CrossRef]
22. Bisplinghoff, R.; Doherty, C. Some studies of the impact of vee wedges on a water surface. *J. Frankl. Inst.* **1952**, *253*, 547–561. [CrossRef]
23. Ahmed, M.R.; Takasaki, T.; Kohama, Y. Aerodynamics of a NACA4412 Airfoil in Ground Effect. *AIAA J.* **2007**, *45*, 37–47. [CrossRef]
24. Qu, Q.; Wang, W.; Liu, P.; Agarwal, R.K. Airfoil Aerodynamics in Ground Effect for Wide Range of Angles of Attack. *AIAA J.* **2015**, *53*, 1048–1061. [CrossRef]
25. Hao, W.; Teo, C.J.; Khoo, B.C.; Goh, C.J. Aerodynamic and stability characteristics of NACA4412 in ground effects. *Int. J. Intell. Unmanned Syst.* **2013**, *1*, 145–153. [CrossRef]
26. Haode, H.; Dongli, M. Airfoil Aerodynamics in Proximity to Wavy Ground for a Wide Range of Angles of Attack. *Appl. Sci.* **2020**, *10*, 6773.
27. Bhatt, P.; Goe, A. Carbon Fibres: Production, Properties and Potential Use. *Mater. Sci. Res. India* **2017**, *14*, 52–57. [CrossRef]
28. Kingston, J. Everything you always wanted to know about Syntactic Foam but were afraid to ask. In Proceedings of the 5th Submarine Science, Technology and Engineering Conference, Fremantle, Australia, 18–22 November 2019; pp. 53–58.
29. Swidan, A.; Thomas, G.; Ranmuthugala, D.; Amin, W.; Penesis, I.; Allen, T.; Battley, M. Experimental drop test investigation into wetdeck slamming loads on a generic catamaran hullform. *Ocean Eng.* **2016**, *117*, 143–153. [CrossRef]
30. Swidan, A.; Thomas, G.; Penesis, I.; Ranmuthugala, D.; Amin, W.; Allen, T.; Battley, M. Wetdeck slamming loads on a developed catamaran hullform—experimental investigation. *Ships Offshore Struct.* **2017**, *12*, 653–661. [CrossRef]
31. Specialist Committee on CFD in Marine Hydrodynamics. Practical Guidelines for Ship CFD Application. In Proceedings of the 26th International Towing Tank Conference, Rio de Janeiro, Brazil, 28 August–3 September 2011.
32. Koshizuka, A.; Oka, Y. Numerical analysis of breaking waves using the moving particle semi-implicit method. *Int. J. Numer. Methods Fluids* **1998**, *26*, 751–769. [CrossRef]
33. Aly, A.M.; Nguyen, M.T.; Lee, S.-W. Numerical analysis of liquid sloshing using the incompressible smoothed particle hydrodynamics method. *Adv. Mech. Eng.* **2015**, *7*, 765741. [CrossRef]
34. Asai, M.; Aly, A.M.; Sonoda, Y.; Sakai, Y. A stabilized incompressible SPH method by relaxing the density invariance condition. *J. Appl. Mathe.* **2012**, *2012*, 139583. [CrossRef]
35. Aly, A.M.; Asai, M.; Chamkha, A.J. Analysis of unsteady mixed convection in lid-driven cavity included circular cylinders motion using an incompressible smoothed particle hydrodynamics method. *Int. J. Numer. Methods Heat Fluid Flow* **2015**, *25*, 2000–2021. [CrossRef]
36. Aly, A.M.; Asai, M. Modelling of non-Darcy flows through porous media using extended incompressible smoothed particle hydrodynamics. *Numer. Heat Transf. Part B Fundam.* **2015**, *67*, 255–279. [CrossRef]
37. Swidan, A.; Amin, W.; Ranmuthugala, D.; Thomas, G.; Penesis, I. Numerical prediction of symmetric water impact loads on wedge shaped hull form using CFD. *World J. Mech.* **2013**, *3*, 311. [CrossRef]
38. Hiemcke, C. Design of a Wing Section in Ground Effect: Application to High Speed Ground Transportation. Ph.D. Thesis, Iowa State University, Ames, IA, USA, 1994.
39. Savitsky, D. Hydrodynamic Design of Planing Hulls. *Mar. Technol. SNAME News* **1964**, *1*, 71–95. [CrossRef]
40. Goddard, R.; Eastgate, J. *Submersible Aircraft Concept Design Study*; Defense Technical Information Centre: Fort Belvoir, VA, USA, 2010; Available online: <https://apps.dtic.mil/sti/citations/ADA554344> (accessed on 1 July 2023).
41. White, A. Water Insertion Options for Special Forces. *Mil. Technol.* **2019**, *43*, 48–49.
42. Nebylov, A.; Nebylov, V. Wing-in-ground effect vehicles flight automatic control systems development problems. *Appl. Me-Chanics Mater. (AEROTECH V Progress. Aerosp. Res.)* **2014**, *629*, 370–375. [CrossRef]
43. Kosari, A.; Chamanpara, H. Investigation of longitudinal dynamics of a small WIG craft in flight over sea Waves. *Ocean Eng.* **2016**, *127*, 23–31. [CrossRef]
44. Matdaud, Z.; Zhahir, A.; Pua’at, A.A.; Hassan, A.; Ahmad, M. Stabilizing Attitude Control for Mobility of Wing in Ground (WIG) Craft—A Review. *IOP Conf. Ser. Mater. Sci. Eng.* **2019**, *642*, 12005. [CrossRef]

45. Wang, L.; Yang, K.; Yue, T.; Liu, H. Wing-in-ground craft longitudinal modeling and simulation based on a moving wavy ground test. *Aerosp. Sci. Technol.* **2022**, *126*, 107605. [[CrossRef](#)]
46. Zhi, H.; Xiao, T.; Deng, S.; Tong, M.; Chen, P.; Wu, B. Distinct Wing-in-Ground Effect of Airfoil in Proximity to Water Waves. *AIAA J.* **2022**, *60*, 3789–3804. [[CrossRef](#)]
47. Seif, M.S.; Dakhrabadi, M.T. A practical method for aerodynamic investigation of WIG. *Aircr. Eng. Aerosp. Technol.* **2016**, *88*, 73–81. [[CrossRef](#)]
48. Dakhrabadi, M.T.; Seif, M.S. Influence of main and outer wings on aerodynamic characteristics of compound wing-in-ground effect. *Aerosp. Sci. Technol.* **2016**, *55*, 177–188. [[CrossRef](#)]
49. Park, K.; Lee, J. Influence of endplate on aerodynamic characteristics of low-aspect-ratio wing in ground effect. *J. Mech. Sci. Technol.* **2008**, *22*, 2578–2589. [[CrossRef](#)]
50. Dakhrabadi, T.M.; Seif, M.S. Hydro-aerodynamic mathematical model and multi-objective optimization of wing-in-ground effect craft in take-off. *Proc. Inst. Mech. Eng. Part M J. Eng. Marit. Environ.* **2018**, *232*, 421–433. [[CrossRef](#)]
51. De Andrade, L.A.; Santos, L.S.C.D.; Gama, A.M. Analysis of radar cross section reduction of fighter aircraft by means of Computer Simulation. *J. Aerosp. Technol. Manag.* **2014**, *6*, 177–182. [[CrossRef](#)]
52. Wang, J.; Ye, J.; Hua, G. Radar cross section statistical characteristics of stealth aircraft using the Weibull-generalized gamma mixture model. *Microw. Opt. Technol. Lett.* **2022**, *64*, 1500–1506. [[CrossRef](#)]
53. Chung, S.-S.M.; Chou, Y.-H.; Chuang, Y.-C. Radar cross section analysis of stealth fighter design: Key factors and limitations of simulation. *Int. J. Electr. Eng.* **2016**, *23*, 201–214. [[CrossRef](#)]
54. Lu, S.; Huang, J.; Yi, M. Study on zonal coating design of absorbing material for a stealth helicopter. *Aircr. Eng.* **2020**, *92*, 1011–1017. [[CrossRef](#)]
55. Shipman, M. How a Tougher Skin Could Change the Shape of Stealth Aircraft. M2 Presswire, 18 May 2021. Available online: <https://news.ncsu.edu/2021/05/tougher-skin-for-stealth-aircraft/> (accessed on 1 July 2023).
56. Dulabhai, H.P.; Raj, A.; Deshpande, P.R.; Thejaraju, R.R.; Shivakumar, S.S.; Santhosh, N.N. A review of buoyancy driven underwater gliders. In *AIP Conference Proceedings*; AIP Publishing: Long Island, NY, USA, 2022; Volume 2421.
57. Latifah, A.; Fatimah, D.D.S.; Hakim, B.L.; Mauluddin, Y. Steering control design and simulation of hybrid underwater glider. *J. Phys. Conf. Ser.* **2019**, *1402*, 44019. [[CrossRef](#)]
58. Lidtke, A.K.; Turnock, S.R.; Downes, J. Characterizing Influence of Transition to Turbulence on the Propulsive Performance of Underwater Gliders. *J. Ship Res.* **2019**, *63*, 198–205. [[CrossRef](#)]
59. Yaxley, K.J.; Joiner, K.F.; Abbass, H.; Bogais, J. Life-learning of smart autonomous systems for meaningful human-autonomy teaming. In *A Framework for Human System Engineering: Applications and Case Studies*; Handley, H., Tolk, A., Eds.; IEEE Wiley: Hoboken, NJ, USA, 2020; pp. 43–61.

Disclaimer/Publisher’s Note: The statements, opinions and data contained in all publications are solely those of the individual author(s) and contributor(s) and not of MDPI and/or the editor(s). MDPI and/or the editor(s) disclaim responsibility for any injury to people or property resulting from any ideas, methods, instructions or products referred to in the content.